Polym. Bull. (2012) 68:2131–2144
DOI 10.1007/s00289-012-0709-y

ORIGINAL PAPER

Star-branched cationic light-emitting dot with silsesquioxane core, synthesis, and light scattering studies

Yang Xiao · Khine Y. Mya · Beng H. Tan · Chao B. He

Received: 18 October 2011 / Revised: 30 December 2011 / Accepted: 17 January 2012 /
Published online: 29 January 2012

Abstract Novel star-like hydrophobic (**M**) and hydrophilic (**W**) hybrid light-emitting dots were synthesized by grafting conjugated arms at eight vertexes of polyhedral oligomeric silsesquioxane (POSS) cage. The water-soluble cationic polymer **W** contains POSS as a core and two layers shell—an inner layer shell consists of the conjugated organic chain and a long chain of hydrophilic polymer as outer layer shell for solubilization in water. The 3D structure renders non-aggregation properties of **W** in solution as the wavelength for the absorption and luminescence spectra remains unchanged over different concentrations. The effects of ionic strength and pH on the properties of cationic polymer **W** were studied using UV, dynamic- and static-light scattering (DLS and SLS).

Keywords Silsesquioxane · Light-emitting · Dot · Cationic · Water soluble · Light scattering

Introduction

Water-soluble conjugated polymers are frequently used as biosensor materials due to their high sensitivity in optical and conductive properties in the presence of analytes [1]. However, aggregation caused by intermolecule and intramolecule aromatic π–π stacking commonly exist in 1D chain-like and 2D disk-like polyelectrolyte [2], which adversely reduces the quantum efficiency of light-emitting applications due to the

Y. Xiao · K. Y. Mya · B. H. Tan · C. B. He (✉)
Institute of Materials Research and Engineering (IMRE) Agency for Science, Technology and Research (A*STAR), 3, Research Link, Singapore 117602, Singapore
e-mail: cb-he@imre.a-star.edu.sg

C. B. He
Department of Materials Science and Engineering, National University of Singapore, Singapore 117576, Singapore

increase in non-radiative emission. Aggregation also results in unstable luminescence, e.g., red-shifted emission from solutions of different concentration [3]. Polyelectrolyte solution is rather complicated due to the strong long-range electrostatic interactions and the dissociation of polyelectrolyte into numerous counter ions and polyions. The aggregation of conjugated polyelectrolyte solution depends on the polymer concentration, salt concentration, solution pH, and polymer charge density. The changes in solvent environment, ionic strength, and temperature have a significant impact on the coil size, aggregation, and the structure of the polymer because of its polyelectrolyte character [4–7].

Recent study on POSS containing light-emitting materials has demonstrated the effectiveness of 'star-like' (3D) structure in improving the quantum efficiency of the light-emitting materials via reducing aromatic π–π stacking [8]. The incorporation of the POSS with conjugated polymer provides a new approach to the preparation of organic light-emitting diodes with improved optoelectronic properties [9]. Recently, our group developed highly luminescent organic quantum dot clusters and polymers using POSS core [10–14]. The organic cluster composed of POSS and organic peripheries (conjugated chains) attached to the eight corners of the core. The incorporation of the organic functional groups onto the POSS core could prevent the conjugated arms from association.

In this article, the design and synthesis of water-soluble spherical core/shell 3D hybrid materials, along with its optical and light scattering properties is reported. Furthermore, the effect of ionic strength and pH on the behavior of the cationic polymer was also investigated.

Experimental section

Materials

Triethylamine, 2-bromoisobutyryl bromide (BiBB), CuCl, 2-dimethylaminoethyl methacrylate (DMAEMA) (98%), 1,1,4,7,10,10-hexamethyltriethylenetetramine (HMTETA), 1,2-dichloromethane (99.9%), methyl iodide (CH_3I), Magnesium (Mg), tetrakis(triphenyl phosphine) palladium (0) were obtained from Sigma-Aldrich and were used as received. *N*–*N*-Dimethylformamide (DMF) (99%, TEDIA), *o*-dichlorobenzene (ODCB) (99%, Merck), and toluene (99.5%, Merck), chloroform ($CHCl_3$, 98%, TEDIA), tetrahydrofuran (THF, 98%, TEDIA) were distilled from calcium hydride (CaH_2). Octa-bromophenyl substituted POSS (**A**) [10] and 2-bromo-3,3′-di-(2-thylhexyl)-2,2′-bithiophene [14] were obtained from our previous work.

Synthesis of 3,3′-di-(2-thylhexyl)-2,2′-bithiophene substituted POSS (Sample **M**)

A Grignard reagent prepared from 2-bromo-3,3′-di-(2-ethylhexyl)-2,2′-bithiophene (4.8 g, 10 mmol) and Magnesium (Mg) (0.29 g, 12 mmol) in 50 ml THF was added dropwise to a solution of Octa-bromophenyl substituted POSS (**A**) (1.672 g,

1 mmol) and tetrakis(triphenyl phosphine) palladium (0) in 20 ml THF at room temperature, and reflux for 24 h. The reaction was quenched by 0.2 M HCl. The mixture was extracted with diethyl. The product was obtained after the mixture was passed through a silica gel column as a viscous liquid with yield of 35%. ^{1}H NMR ($CDCl_3$, 400 MHz, δ ppm): 8.120 (m, 1H, Si–C_6H_4–), 7.618 (m, 1H, Si–C_6H_4–), 7.551 (m, 1H, Si–C_6H_4–), 7.402 (m, 1H, Si–C_6H_4–), 7.325 (m, 1H, –C_4H_2S), 6.964 (m, 2H, –C_4HS, –C_4H_2S), 2.444 (m, 4H, –CH_2–), 1.538 (m, 2H, –CH–), 1.188 (m, 16H, –CH_2–), 0.914 (m, 12H, –CH_3). ^{13}C NMR ($CDCl_3$, 400 MHz, δ ppm): 143.826 (–C_6H_4–Si–), 143.341 (–C_4HS–), 142.907 (–C_4HS, –C_4H_2S–), 142.807 (–C_4H_2S–), 135.306 (–C_6H_4–), 133.951 (–C_6H_4–), 131,102 (–C_6H_4–), 130.670 (–C_6H_4–), 129.438 (–C_4HS–), 128.829 (–C_4H_2S–), 127.419 (–C_6H_4–), 125.876 (–C_4HS–), 125.799 (–C_4H_2S–). ^{29}Si NMR ($CDCl_3$, 400 MHz, δ ppm): −69.619. GPC: M_w 4200, M_n 4090, $M_w/M_n = 1.03$. FTIR: 2938, 2917, 2850 (υ–C–H), 1452, 1374 (υ=C–H), 1108 (υ–Si–O–Si), 813 (υ=C–H).

Synthesis of quaternized POSS-(phenyl-bithiophene-PDMAEMA)$_8$ (**W**)

The general synthesis procedure is as follow: 10 mmol *n*-BuLi (1.6 M solution in Hexane, 6.25 ml) was added into a solution of **M** (4.14 g, 1 mmol) in dry THF 40 ml at −78 °C under stirring. After stirring for two hrs at −78 °C, CO_2 was passed into the mixture from dry ice. The flow of CO_2 was allowed to continue overnight and gradually warmed to room temperature. Subsequently, the mixture was poured into a cooled 1 M HCl solution (with ice) and the aqueous solution was extracted twice with chloroform. The combined extracts were washed with water and dried over anhydrous MgSO4. The 3,3′ Di-(2-thylhexyl)-5-carboxy-2,2′-bithiophene substituted POSS-phenyl (**M-COOH**) was obtained from the mixture with a yield of 65% after passing through a silica column. The obtained **M-COOH** (3.8 g, 0.85 mmol) in a solution of 20 ml ether was added drop wise into $LiAlH_4$ (15 mmol, 0.57 g) solution of ether (70 ml) under reflux and remained stirring at this temperature for 4 h. The reaction mixture was then added into cold 0.1 M HCl 30 ml (with ice), and the organic phase was separated and washed using water while the solvent was removed by distillation. The mixture was passed through a silica column and the yield of **M-OH** obtained is 75%. Subsequently. **M-OH** was converted to the final product according to the procedures proposed by Lu et al. [17]. The solution of **M-OH** (0.5 g, 0.117 mmol) and triethylamine (4.4 ml, 31 mmol) in dry CH_2Cl_2 (40 ml) was added drop wise into 2-bromoisobutyryl bromide (BiBB) (3.6 ml, 26 mmol) at 0 °C under Ar atmosphere, followed by stirring at room temperature over night. The organic phase was passed through a short silica column using toluene as eluent and the microinitiator (N) was obtained with yield of 25%. In a glass tube, 0.07 g (0.0125 mmol) of microinitiator (N) and 0.01 g of CuCl (0.1 mmol) was charged, sealed, degassed and filled with Ar followed by the addition of *o*-dichlorobenzene (1.2 ml) and 1,1,4,7,10,10-hexamethyltriethylenetetramine (HMTETA) (0.0268 ml, 0.1 mmol). The glass reactor was immersed in an oil bath at 90 °C, and a clear solution with light green color formed within a few seconds. Upon dissolution, 2.21 ml of 2-(dimethylamino)ethyl methacrylate (DMAEMA) (13.26 mmol) was quickly injected into the tube to carry out the polymerization. Two hours later the polymer was passed

through a silica column to remove the catalysts and precipitated in excess of hexane followed by drying in a vacuum oven at 40 °C. The light yellow product was dissolved in 50 ml of dry THF followed by the addition of methyl iodide (methyl iodide/DMAEMA as 2:1) and stirred overnight at room temperature. The light yellow precipitate was collected and washed with THF. The sample was dried and a light yellow crystalline **W** was obtained (yield > 90%) which is soluble only in water. ^{1}H NMR (D_2O, ppm) 4.5(s, O–CH_2–), 3.8(s, N–CH_2–), 3.26[s, N–$(CH_3)_4$], 1.8[s, CH_2–$C(CH_3)$], 1.0(s, C–CH_3). Elemental analysis: Calculation for **W** (**M**-$[C_5H_8O_2$–$(C_9H_{18}O_2NI)_{132}]_8$) (according to feed ratio) C, 36.6; H, 6.1; N, 4.6, Found, C, 35.3; H, 6.3; N, 4.7.

Characterization

^{1}H, ^{13}C, ^{29}Si nuclear magnetic resonance (NMR) data were obtained using a Bruker Avance 400 spectrometer. Elemental microanalysis was carried out by the Microanalysis Laboratory of the National University of Singapore. Gel permeation chromatography (GPC) analysis was carried out with a Shimadzu SCL-10A and LC-8A system equipped with two Phenogel 5 μ 50 and 1,000 Å columns in series and a refractive detector, using THF as the eluent at a flow rate of 0.3 ml/min at 40 °C. Monodispersed poly(ethylene glycol) were used as standards. UV–Vis spectra were recorded on a Shimadzu 3101 spectrophotometer. Photoluminescence (PL) measurement was carried out on a Perkin-Elmer LS 50B luminescence spectrometer with a xenon lamp as a light source. The concentration of polymers for UV and PL analysis is less than 1×10^{-3} g/ml. The polymer thin films were cast on a quartz plate using a spin coater.

Light scattering studies

Dynamic- and static-light scattering (DLS and SLS) studies [15, 16] were performed using a Brookhaven (BI-200 SM) light scattering instrument. The light source was a 35-mW He–Ne laser emitting vertically polarized light of 632.8 nm wavelength. The intensity measurements were carried out at different scattering angle (30°–130°) to measure the molecular weight (M_w) of copolymer and the radius of gyration (R_g) by SLS. By measuring the optical constant (K) and the excess Rayleigh ratio (ΔR_θ) in an infinite dilution, the M_w, R_g, and the second viral coefficient (A_2) can be determined by the extrapolation of $Kc/\Delta R_\theta$ to zero angle and zero concentration according to the relation

$$\frac{Kc}{\Delta R_\theta} = \frac{1}{M_w}\left[1 + \frac{16\pi n^2}{3\lambda^2} R_g^2 \sin^2\left(\frac{\theta}{2}\right)\right] + 2A_2 c \qquad (1)$$

where K is the optical constant, which depends on the refractive index increment of the polymer solution ($K = 4\pi^2 n^2 (\mathrm{d}n/\mathrm{d}c)^2 / N_A \lambda^4$). Here, $\mathrm{d}n/\mathrm{d}c$ is the refractive index increment of the polymer solution, N_A being the Avogadro's number, and ΔR_θ is the excess Rayleigh ratio [$\Delta R_\theta = R_\theta$(solution) − R_θ(solvent)], respectively. The second viral coefficient (A_2) describes the polymer–solvent interaction. The light

scattering studies were carried out at 25 °C in the polymer concentrations range 1–4 mg/ml in aqueous solution with added salt (0.01 and 0.1 M NaCl). Before both DLS and SLS measurements, all the solvents were filtered through 0.2 μm Millipore membrane filters (Whatman) to remove dust particles and the solutions were centrifuged at 8,000 rpm for 30 min and then filtered with 0.22 μm Millipore filters directly into the light scattering cell. The dn/dc at constant chemical potential, $(\mathrm{d}n/\mathrm{d}c)_{\mu}$, for each solution was determined using a Brookhaven differential refractometer at a wavelength of 620 nm and the instrument was calibrated using solution of potassium chloride (KCl). Before measurement, the polymer solutions were dialyzed against the salt solution for 2 days. The dn/dc was then measured at constant solvent chemical potential by comparing the refractive index of the dialyzed solution with the solvent.

Results and discussion

Scheme 1 described the synthesis approach for the water-soluble light-emitting dot. The spherical compound **M** was synthesized via Palladium-catalyzed coupling reaction following the procedure described in our previous work [10]. **W** was obtained by subsequent water-solubilizing reactions [17] from **M**. The thickness of water-soluble layer, and thus the size of the light-emitting dots could be easily controlled by the feeding ratio of starting materials. Compound **M** has only one sharp peak in ^{29}Si NMR at–69.619, slightly different from oligophenylene substituted POSS materials [10], indicating that the POSS cage structure remains intact after the reaction. It is worth to mention **W** is highly soluble in water, just like conventional inorganic salts, which could be used in biological environment.

Photoluminescent spectra of **M** in condense state (film) and dilute solution are shown in Fig. 1. In contrast to the conventional light-emitting materials, the spectrum of solid film did not red-shift from that of solution. The non-red-shifting feature of **M** implies that the unique molecular structure of **M** prevents intermolecular aggregation. This could be attributed to highly branched alkyl chains on the outer layer of the light-emitting dot which prevent intramolecule π–π stacking due to a rigid frame of POSS.

Absorption and photoluminescence (PL) studies of **W** in water are shown in Fig. 2. The emission wavelength of **W** (λ_{max}448 nm) in water is, however, red-shifted from **M** (λ_{max}410 nm) in THF. Our previous study showed that the higher polarity of the solvent could lead to red-shift of PL spectrum [12]. The UV absorption and PL spectra are remaining at same wavelength when changing concentration of the water solution of **W**. It is interesting to note that after attaching water-soluble chain on the end of conjugated chain, this non-aggregation property of **M** has remained onto **W**. It is reported that the conjugated polyelectrolyte undergoes conformational changes that accompany aggregation in aqueous solution [18–20]. The decrease in the fluorescence quantum yield and emission energy suggests that this aggregate fluorescence is dominated by interchain excimer type emission [18–20]. The newly synthesized molecule **W** shows non-aggregation property that is better than conventional conjugated polyelectrolyte. Our star-like 3D molecular

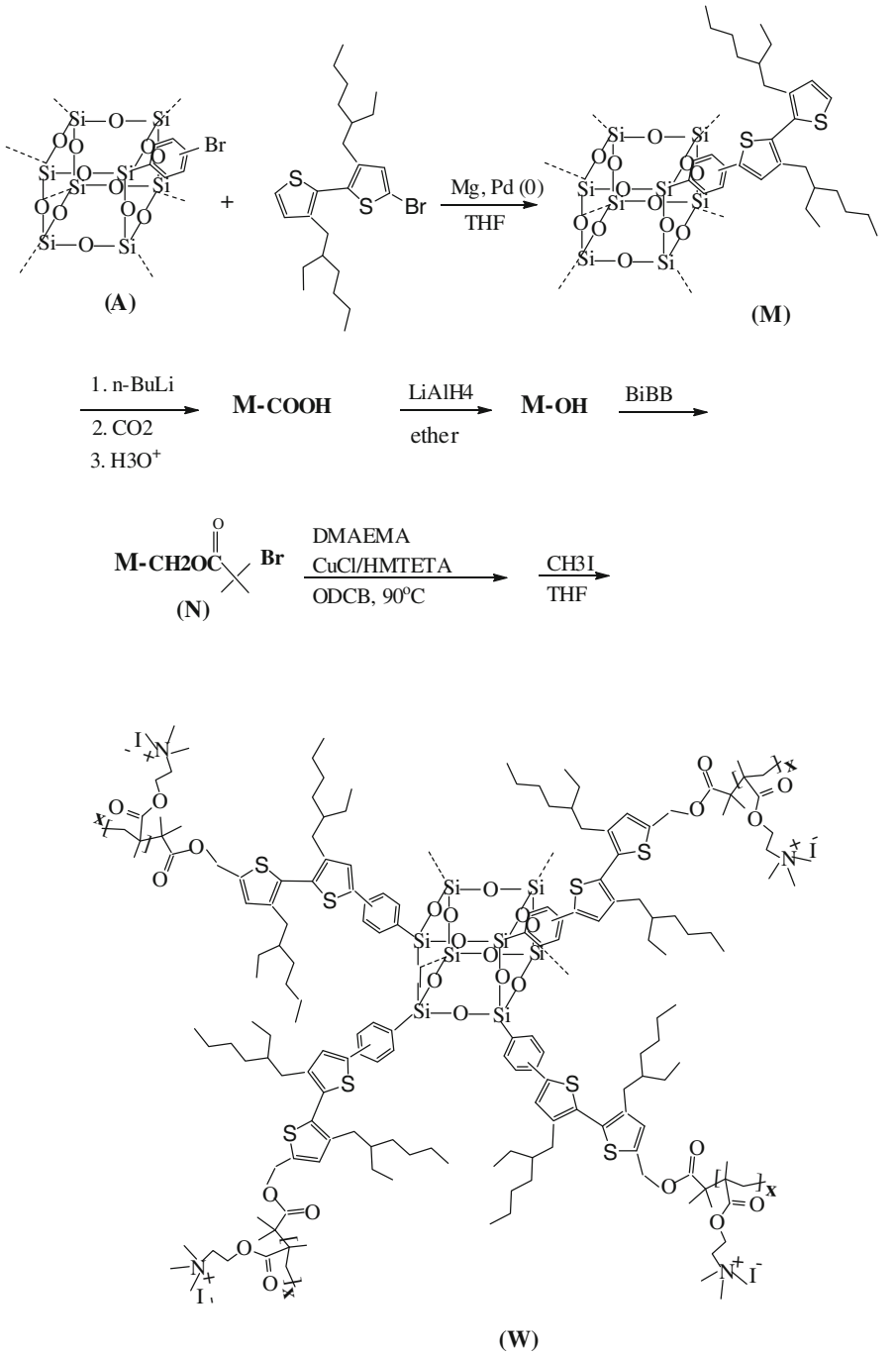

Scheme 1 Synthesis of hydrophobic dot **M** and hydrophilic dot **W**

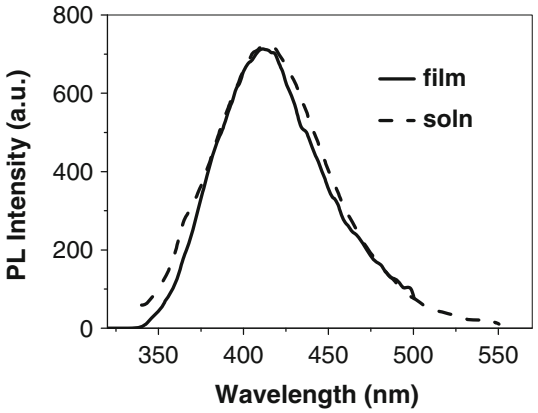

Fig. 1 Photoluminescent of **M** in film and THF solution (10^{-3}g/ml)

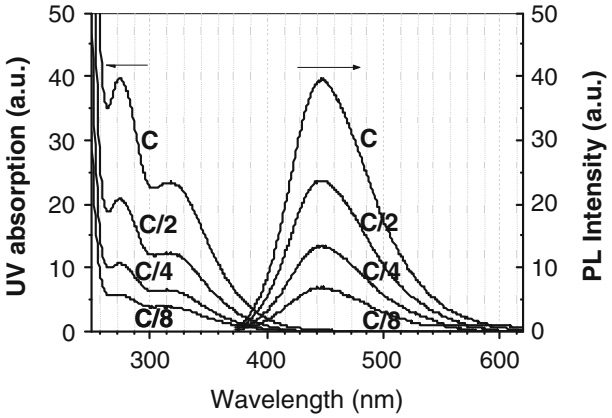

Fig. 2 Absorption UV and PL spectra of **W** in aqueous solution at different concentrations. Concentration *C* is 2 mg/ml, *C/2* is 1 mg/ml, *C/4* is 0.5 mg/ml, *C/8* is 0.25 mg/ml

structure has advantage over linear polymer chain in this regard. One should raise the question that is this non-shifting feature of **W** in water solution due to electrostatic repulsion of the polyelectrolyte? The electrostatic repulsion of the polyelectrolyte may help to reduce the aggregation of charge-carrying luminescent chains in some extent, but it can't eliminate interchain π–π stacking completely. There are reported polyelectrolyte systems showing severe aggregation and spectrum shifting following concentration of solution changing [18–20].

The optical properties of **W** were studied in aqueous solution at different pH value, as shown in Fig. 3. UV spectra of **W** in different pH solution indicate that the absorption is quite stable against pH changing. Strong acid (pH $<$ 3) results in the red-shift of the UV spectrum of **W** while weak acid and base environment does not shift the wavelength. In contrast to UV spectrum, strong acid results in the slightly blue-shift of the PL spectrum of **W** while weak acid and base environment does not change the position of the PL spectrum of **W**. Figure 3 shows that strong acid will

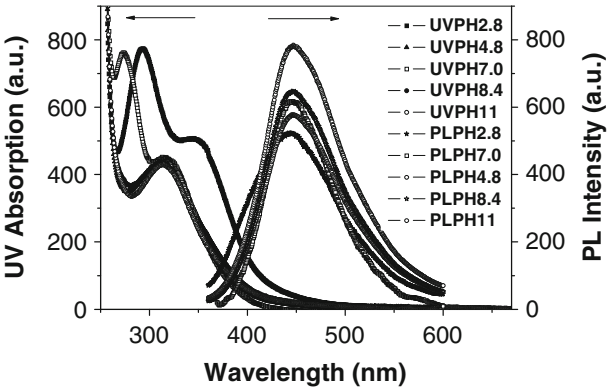

Fig. 3 Normalized UV and original PL spectra of **W** in aqueous solution with different pH value. The solution concentration is 3 mg/4 ml

reduce the intensity of the emission while base solution will enhance the intensity. Just like attaching electron withdrawing group onto conjugated chain normally will reduce its luminescent intensity and grafting electron donating group will enhance emission intensity, protons decrease the electron density of emissive chains hence reduce the luminescent intensity of **W** and basic groups increase electron density of emissive chains therefore enhance luminescent intensity of molecule **W**. The large amount of protons would have impact to the conformation change of conjugated chains such as protons reduce electrostatic repulsion of hydrophilic chains onto that there are many ester groups. The closer packing of hydrophilic chains in acid solution, compare to the packing in neutral environment, caused by protons/hydrogen-bond may lead conformation changes of conjugated chains therefore the UV spectrum pattern is different from that in weak acid and weak base solution as well as λ_{max} red-shifts. However, the on-set of all UV absorption spectra, including the spectrum in strong acid, are similar hence the emissive wavelength of PL spectra in varied PH solution are similar.

The distribution of hydrodynamic radius (R_h) of **W** in aqueous solution, obtained from dynamic light scattering measurement, is shown in Fig. 4. The distribution is

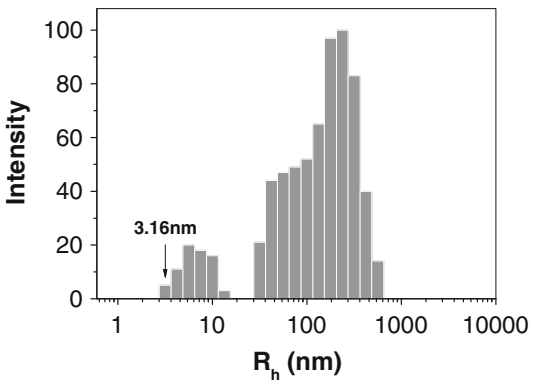

Fig. 4 Hydrodynamic radius (R_h) distribution of **W** in aqueous solutions, measured at 90°. The concentration is 1.3 mg/ml

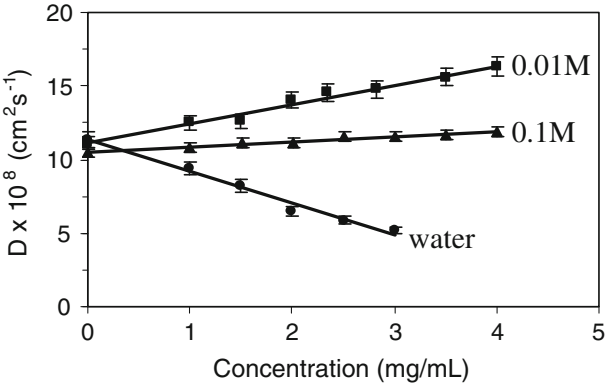

Fig. 5 The diffusion coefficients of sample **W** in aqueous solution and in the presence of salt, 0.01 and 0.1 M NaCl solutions. The concentration of sample **W** is 2 mg/ml measured at 25 °C

bimodal where the fast mode ($R_h \sim 6$ nm) corresponds to the size of individual molecule **M** and partially grafted with water-soluble molecule, and the slow mode ($R_h \sim 31$–500 nm) corresponds to aggregated molecules due to the long hydrophilic chains having high chances to entangle with each other in concentrated solution. We hypothesize that the association does not take place between the conjugated chains since the aggregation does not affect the emission wavelength as proven in Fig. 2.

Figure 5 demonstrate that the fast diffusion coefficient (D_f) of sample **W** in aqueous solution decreases as increasing polyelectrolyte concentration whereas the diffusion coefficients increase in the presence of salt. However, the values of D_0 in salt solutions (0.01 and 0.1 M NaCl) are approximately the same as that in water within the experimental error. With the addition of salt, the hydrodynamic size of the cationic polymer shrinks as the salt screens the electrostatic repulsions and therefore, the diffusion coefficient increases with increasing salt (NaCl) concentration. The increase of diffusion coefficient becomes less pronounced ($D \sim c^{0.35}$) at high ionic strength (0.1 M NaCl) arising from the counterion coupling effect. The isotropic model [21] predicts $D \sim c^{0.5}$ or $\sim c^{0.38}$ depending on the ionic strength.

In Fig. 6, the hydrodynamic radii (R_h) at infinite solutions were determined from the diffusion coefficients of each solution as shown in Fig. 5 via Stoke-Einstein equation; $R_h = k_B T/6\pi\eta_s D_0$, where $k_B T$ is the thermal energy, η_s being the viscosity of the solvent and D_0 is the infinite diffusion coefficient. The R_h of sample **W** both in salt solutions and salt-free aqueous solution are found to be 21. 6 nm (water), 21.1 nm (0.01 M), and 20.7 nm (0.1 M), respectively.

It is extremely challenging to measure Zimm plot to obtain M_w, R_g, and A_2 for polyelectrolyte solution because of its weak scattering and metastable state between dissociation and association of polyelectrolyte in solution. Therefore, SLS measurements were performed in added salt solutions. Figure 7 shows the Zimm plot for sample **W** in 0.01 M NaCl. The extrapolation to zero concentration and zero angle leads to M_w and the slopes of angle and concentration dependence give rise to the radii of gyration (R_g) (30.4 nm) and A_2 (2.4×10^{-4} cm^3 mol/g^2), respectively.

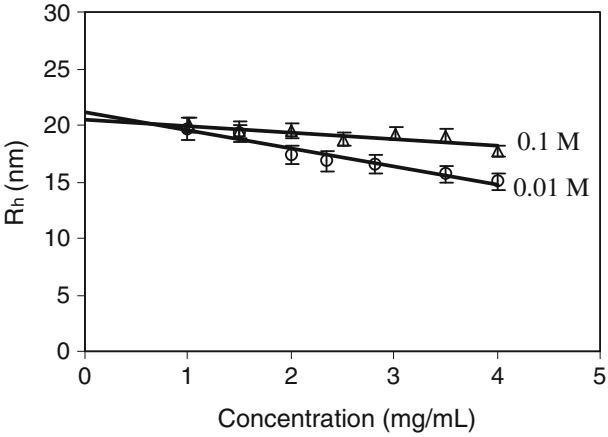

Fig. 6 Hydrodynamic radii (R_h) of **W** in aqueous solution and in the presence of salt, 0.01 and 0.1 M NaCl solutions. The concentration of sample **W** is 2 mg/mL measured at 25 °C

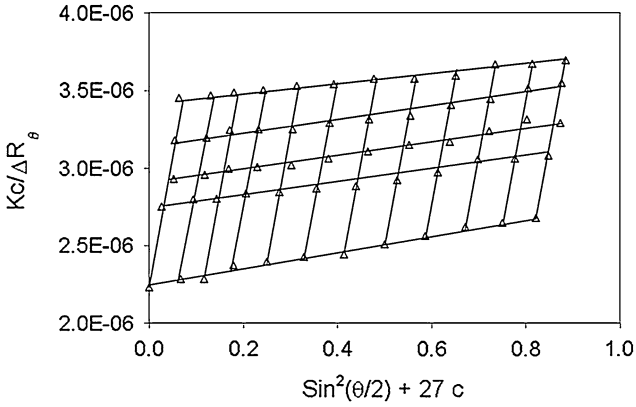

Fig. 7 The Zimm plot analysis for sample **W** in 0.01 M NaCl solution

The Zimm plot indicates that the measured concentration range (1–4 mg/mL) is low enough to avoid the interference effect. Note that this effect leads to upward curvature of $Kc/\Delta R_\theta$ versus polyelectrolyte concentration [22]. The positive value of A_2 indicates the polyelectrolyte in good solvent. The variations of R_g with added salt are reported in Table 1 which decreases with added salt, following the same trend as the decrease in R_h. The M_w of sample **W** in different ionic strength were also determined by viscosity measurement in comparison to the results obtained by light scattering studies. Assuming the sample **W** as a spherical particle, M_w can be calculated according to the relation

$$M_w = \frac{2.5N_A}{[\eta]}\left(\frac{4}{3}\pi R_h^3\right) \quad (2)$$

Table 1 The physical parameters of sample **W** in different salt concentration studied by light scattering

Sample **W** in different salt concentration	$(dn/dc)_{\mu}$ (ml/g)	R_h (nm)	R_g (nm)	R_g/R_h	$M_w \times 10^{-5}$ (g/mol)[a]	$M_w \times 10^{-5}$ (g/mol)[b]	A_2 x 10^4 (cm^3 mol/g^2)
0.01 M NaCl	0.1098 ± 2.1	21.1 ± 2.1	30.4 ± 3.3	1.44	4.48 ± 0.04	4.88	2.39 ± 0.82
0.1 M NaCl	0.1035 ± 2.1	20.7 ± 1.4	29.1 ± 1.2	1.41	4.43 ± 0.03	4.82	2.79 ± 0.26

[a] Molecular weight obtained by Zimm plot

[b] Molecular weight determined by the combination of DLS and viscosity measurements

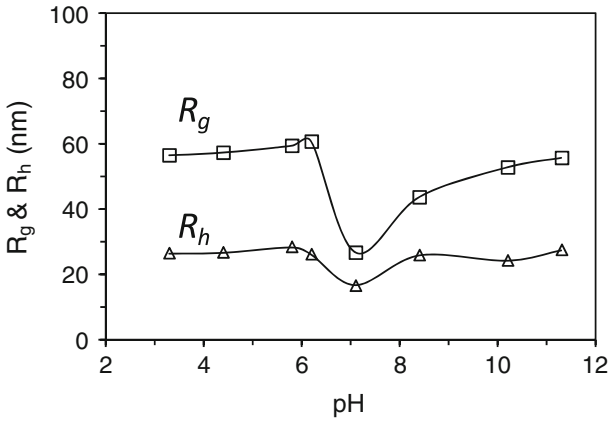

Fig. 8 The dependence of R_g (*upper curve*) and R_h (*lower curve*) on pH value for sample W at 0.01 M NaCl solution. The concentration of sample **W** is 2 mg/mL measured at 25 °C

where η is the intrinsic viscosity, N_A being Avogadro number, and R_h is the hydrodynamic radius obtained by DLS measurement. η was obtained using Huggins plot according to the equation

$$\frac{\eta_{sp}}{c} = [\eta] + K_H[\eta]^2 c \tag{3}$$

where η_{sp}/c is the reduced viscosity, K_H is the Huggins coefficient, and c is the polyelectrolyte concentration. The data are summarized in Table 1.

The value of ρ ($\rho = R_g/R_h$) is estimated to be 1.4 which corresponds to the star-like structure in good solvent with high branching density [23].

Although the solution is in dilute regime, the electrostatic screening effect is important due to the presence of the free counterions in the solution and the compactness of the star-like polymer compared to the linear polymers. The screening effect is usually described by a Debye–Huckel screening length λ_D, related to the presence of free counterions in the solution [7].

Figure 8 shows the effect of pH on the values of R_g and R_h for sample **W** at low ionic strength (0.01 M NaCl). At isoelectric point (pH 7.2), both R_g and R_h exhibit a minimum value. The increase in the net positive charge of cationic polymer via decrease in pH enhances the electrostatic repulsion between polyions leading to a large size at low pH.

Conclusion

Novel spherical hydrophobic (**M**) and hydrophilic (**W**) hybrid light-emitting dots are synthesized via grafting of conjugated arms at eight vertexes of POSS cages. **M** exhibits non-aggregative characteristics leading to identical emission in solid state and in solution as PL spectra of film does not red-shift from that of dilute solution. The hydrophilic star-like emitting dot **W** is highly water-soluble and the

emissive wavelength is stable over a wide range of pH (3–11). The UV and PL wavelengths of **W** in aqueous solution remain unchanged when the concentration of polymer changes. This property is extremely interesting as the emission of **W** will be stable and not affected by changing concentration. Light scattering studies for the cationic polymer indicates **W** may form aggregates in concentrated solution via water-soluble chain tangling but the emissive moiety does not aggregate. The hydrophilic 3D molecule **W** shrinks in the presence of NaCl therefore, the diffusion coefficient increases at high concentration. The effect of pH on the values of R_g and R_h for sample **W** at low ionic strength (0.01 M NaCl) indicates at isoelectric point (pH 7.2), both R_g and R_h exhibit a minimum value. The hydrodynamic radii R_h of sample **W** both in salt solutions and salt-free aqueous solution are found to be approximately 21 nm. The molecular size, R_g and molecular weight, M_w of **W** is approximately 30 nm and 4.5×10^5 g/mol, respectively, in NaCl solution. The new water-soluble light-emitting dot could be potentially used in biosensor applications.

References

1. Liu B, Bazan GC (2006) Synthesis of cationic conjugated polymers for use in label-free DNA microarrays. Nat Protoc 1:1698–1702
2. Liu Y, Ogawa K, Schanze KS (2009) Conjugated polyelectrolytes as fluorescent sensors. J Photoch Photobio C 10:173–190
3. Chen SA, Jen TH, Lu HH (2010) A review on the emitting species in conjugated polymers for photo- and electro-luminescence. J Chin Chem Soc-Taip 57:439–458
4. McQuade DT, Pullen AE, Swager TM (2000) Conjugated polymer-based chemical sensors. Chem Rev 100:2537–2574
5. Stork M, Gaylord BS, Heeger AJ, Bazan GC (2002) Energy transfer in mixtures of water-soluble oligomers: effect of charge, aggregation, and surfactant complexation. Adv Mater 14:361–366
6. Cimrova V, Schmidt W, Rulkens R, Schulze M, Meyer W, Neher D (1996) Efficient blue light emitting devices based on rigid-rod polyelectrolytes. Adv Mater 8:585
7. Baur JW, Kim S, Balanda PB, Reynolds JR, Rubner MF (1998) Thin-film light-emitting devices based on sequentially adsorbed multilayers of water-soluble poly(p-phenylene)s. Adv Mater 10: 1452–1455
8. Lin WJ, Chen WC, Wu WC, Niu YH, Jen AKY (2004) Synthesis and optoelectronic properties of starlike polyfluorenes with a silsesquioxane core. Macromolecules 37:2335–2341
9. Kang JM, Cho HJ, Lee J, Lee JI, Lee SK, Cho NS, Hwang DH, Shim HK (2006) Highly bright and efficient electroluminescence of new PPV derivatives containing polyhedral oligomeric silsesquioxanes (POSSs) and their blends. Macromolecules 39:4999–5008
10. He CB, Xiao Y, Huang JC, Lin TT, Mya KY, Zhang XH (2004) Highly efficient luminescent organic clusters with quantum dot-like properties. J Am Chem Soc 126:7792–7793
11. Xiao Y, Liu L, He CB, Chin WS, Lin TT, Mya KY, Huang JC, Lu XH (2006) Nano-hybrid luminescent dot: synthesis, characterization and optical properties. J Mater Chem 16:829–836
12. Xiao Y, Tripathy S, Lin TT, He CB (2006) Absorption and Raman study for POSS-oligophenylene nanohybrid molecules. J Nanosci Nanotechnol 6:3882–3887
13. Xiao Y, Lu XH, Tan LW, Ong KS, He CB (2009) Thermally stable red electroluminescent hybrid polymers derived from functionalized silsesquioxane and 4,7-bis(3-ethylhexyl-2-thienyl)-2,1,3-benzothiadiazole. J Polym Sci Pol Chem 47:5661–5670
14. Xiao Y, Lu XH, Zhang XH, He CB (2010) Synthesis and optical characteristics of organic light-emitting dot based on well-defined octa-functionalized silsesquioxane. J Nanopart Res 12:2787–2798
15. Brown W (1996) Light scattering: principles and development. Clarendon Press, Oxford
16. Radeva T (2001) Physical chemistry of polyelectrolytes 99. Marcel Dekker, Inc., New York

17. Lu S, Fan QL, Chua SJ, Huang W (2003) Synthesis of conjugated—ionic block copolymers by controlled radical polymerization. Macromolecules 36:304–310
18. Kim J, Swager TM (2001) Control of conformational and interpolymer effects in conjugated polymers. Nature 41:1030–1034
19. Levitus M, Schmieder K, Ricks H, Shimizu KD, Bunz UHF, Garcia-Garibay MA (2001) Steps to demarcate the effects of chromophore aggregation and planarization in poly(phenyleneethynylene)s. 1. Rotationally interrupted conjugation in the excited states of 1,4-bis(phenylethynyl)benzene. J Am Chem Soc 123:4259–4265
20. Walters KA, Ley KD, Schanze KS (1999) Photophysical consequences of conformation and aggregation in dilute solutions of pi-conjugated oligomers. Langmuir 15:5676–5680
21. Odijk T (1979) Possible scaling relations for semidilute polyelectrolyte solutions. Macromolecules 12:688–693
22. Huglin MB (1972) Light scattering from polymer solutions. Academic Press, London
23. Smith AD, Shen CKF, Roberts SR, Helgeson R, Schwartz BJ (2007) Ionic strength and solvent control over the physical structure, electronic properties and superquenching of conjugated polyelectrolytes. Res Chem Intermed 33:125–142